Supplemental Materials for "First-principles spin-transfer torque in room temperature ferromagnet 2D van der Waals magnetic tunnel junctions"

Masoumeh Davoudiniya[1] and Biplab Sanyal[1,*]

[1] *Department of Physics and Astronomy, Uppsala University, Box-516, 75120 Uppsala, Sweden*

(Dated: October 25, 2024)

CONTENTS

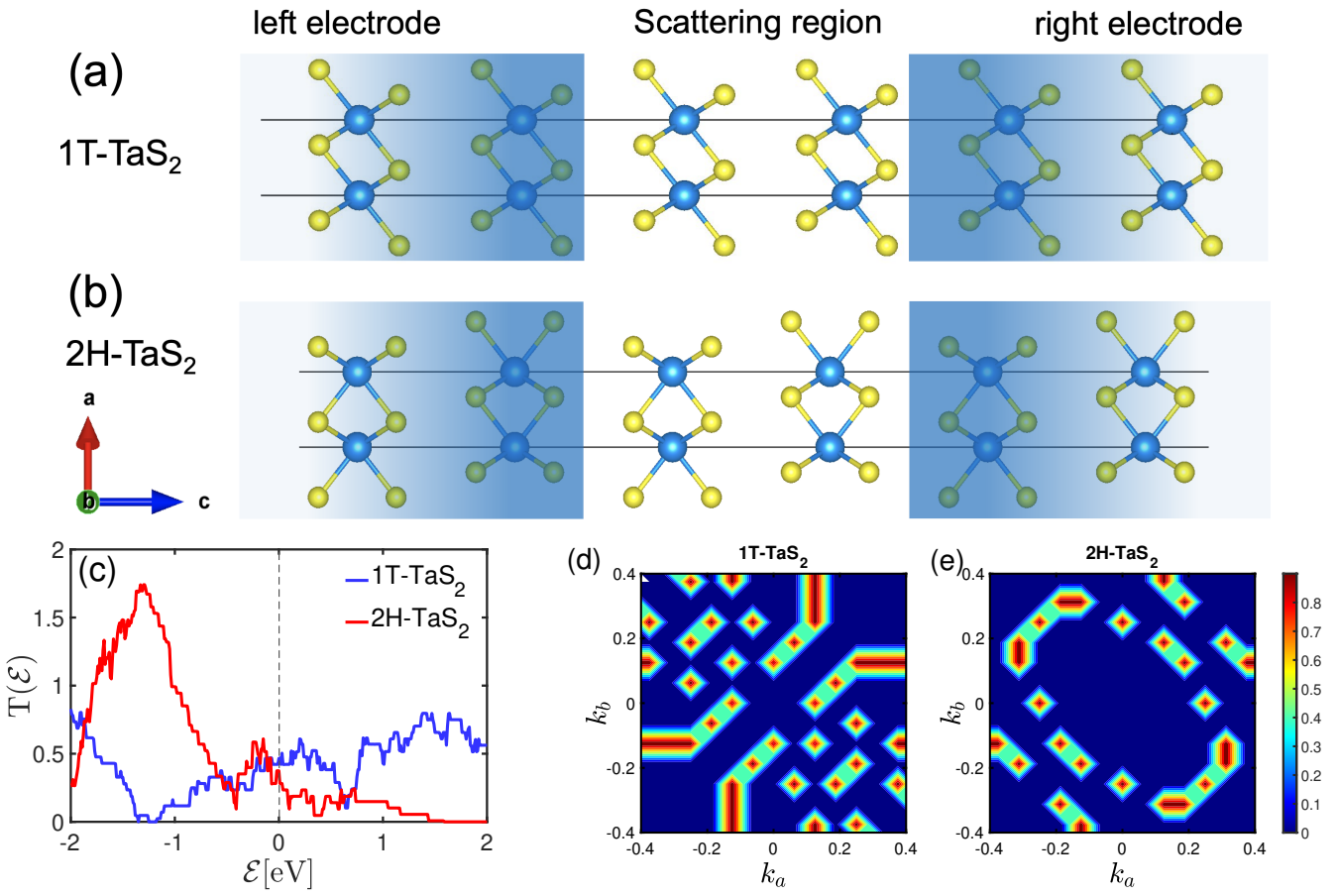

FIG. 1. Two-probe model used for NEGF calculations, depicting a device made of an infinite number of (a) 1T-TaS_2 and (b) 2H-TaS_2 layers. (c) Transmission spectra $T(\mathcal{E})$ for bulk structures of 1T-TaS_2 and 2H-TaS_2 as a function of energy, highlighting the distinct electronic properties of the two phases. $k_{\parallel}$-resolved transmission probability of bulk (d) 1T-TaS_2 and (e) 2H-TaS_2 at the Fermi level.

* Biplab.Sanyal@physics.uu.se

I. TRANSPORT THROUGH BULK STRUCTURES

Figures 1a and 1b present a device made of an infinite number of 1T-TaS_2 and2H-TaS_2 layers, respectively. Fig. 1c illustrates a comparative analysis of the electronic transmission coefficient of bulk 1T-TaS_2 and 2H-TaS_2 phases, which are used as metallic electrodes in our MTJs. Transmission at a given energy is related to the number of available subbands at that particular energy. It is clear that changing the polytype phase of TaS_2 affects the transmission coefficient, as these changes arise from the differences in the electronic band structure and density of states of these materials, as shown in Fig. 1d and Fig. 1e. Although 2H-TaS_2 has a higher DOS at the Fermi level compared to 1T-TaS_2 (see Fig. 1e and Fig. 1d, respectively), the transmission spectrum shows that the probability of transmission for 1T-TaS_2 is higher than for 2H-TaS_2. This discrepancy can be attributed to the fact that a higher DOS at the Fermi level can introduce more scattering mechanisms and localization effects, resulting in less favorable transmission pathways, all of which can reduce the transmission coefficient. Therefore, even though 2H-TaS_2 might have more available electronic states at the Fermi level, the actual transmission depends on a complex interplay of these factors. Figures 1d and 1e show the $k_{\|}$-resolved transmission probability at the Fermi level for bulk 1T-TaS_2 and 2H-TaS_2, respectively. These plots further illustrate the differences in the electronic properties and the impact on the transmission probabilities of the two polytypes.

II. ELECTRONIC PROPERTIES

The band structure of bulk 1T-VSe_2 depicted in Fig. 2 reveals prominent d-orbital contributions for both spin-up and spin-down channels across the high-symmetry points in the Brillouin zone. Panel (a) shows significant dispersion band crossings at the Fermi level for the spin-up channel, primarily influenced by the d_{z^2} orbital, showing metallic behavior. Conversely, panel (b) illustrates that the spin-down channel exhibits less dispersion, with the d_{z^2} orbital closely approaching the Fermi level near the Γ point, potentially impacting the material's transport properties. The distinction in band behavior between the spin channels, especially around the M and K points, underscores the role of spin polarization in shaping the electronic structure. Along the Γ−A direction, which is the transport direction, the d_{z^2} orbital band crosses the Fermi level in the spin-up configuration as shown in panel (b), while in the spin-down channel depicted in panel (b), no bands are observed at the Fermi level, highlighting a difference in transport properties between the two spin states.

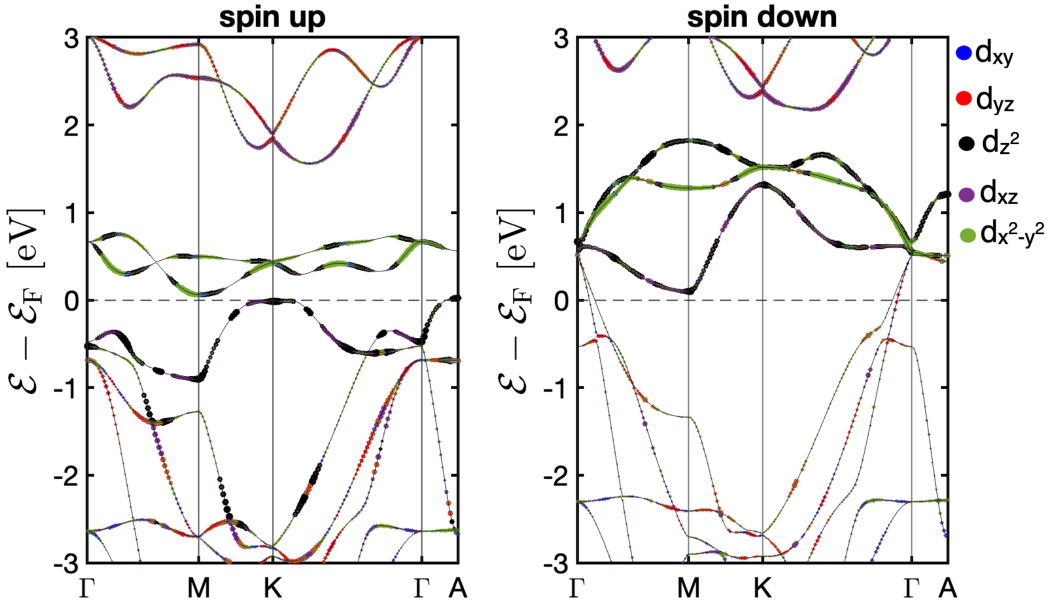

FIG. 2. d-orbital projected band structure 1T-VSe_2 for the spin up and down the channel.

The orbital-projected density of states for a freestanding monolayer of VSe_2 is depicted in Fig.3. It displays distinct spin-up and spin-down states, indicating significant spin polarization. Notably, the d-orbitals exhibit a high density of states at the Fermi level, indicative of metallic properties. This predominance of d-orbital contributions near the Fermi level is characteristic of transition metal dichalcogenides (TMDCs). Conversely, the DOS for bulk VSe_2, shown

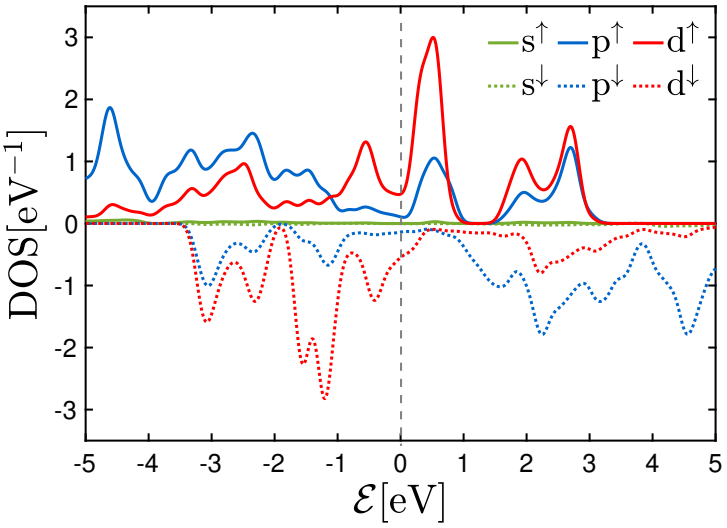

FIG. 3. Orbital-projected DOS of free-standing monolayer VSe_2.

in Fig. 1(f), features sharper and more intense peaks, particularly within the d orbitals. This heightened definition in the bulk form can be attributed to additional electronic interactions inherent to its three-dimensional structure, which contrast with the broader energy levels observed in the monolayer that arise from quantum confinement and surface effects.

The complex band structure methodology extends beyond traditional band structure analyses by including wavevectors with complex components. This advanced approach not only identifies the usual bulk-propagating states but also integrates evanescent states, which exhibit exponential growth or decay between unit cells. Normally disregarded due to the constant translational symmetry of ideal crystals, these states become critical under conditions where this symmetry is interrupted, such as near impurities or at crystal surfaces [1, 2]. Figure 4 shows the complex band structures of bulk 1T-VSe_2, examining both the (a) spin-up and (b) spin-down channels along the out-of-plane $\Gamma - A$ direction of the first Brillouin zone. Each panel distinctly separates the real components of the band structure (depicted on the right side) from the imaginary components (κ_C, depicted on the left side). The parameter L, fixed at 6.35 Å in the context of bulk 1T-VSe_2 with AA stacking, plays a critical role in determining the scale of κ_C, which is instrumental in analyzing the propagation and decay characteristics of wave modes. The evanescent states, characterized by a decay length inversely related to κ_C, are essential for a thorough analysis of wave transmission, especially through

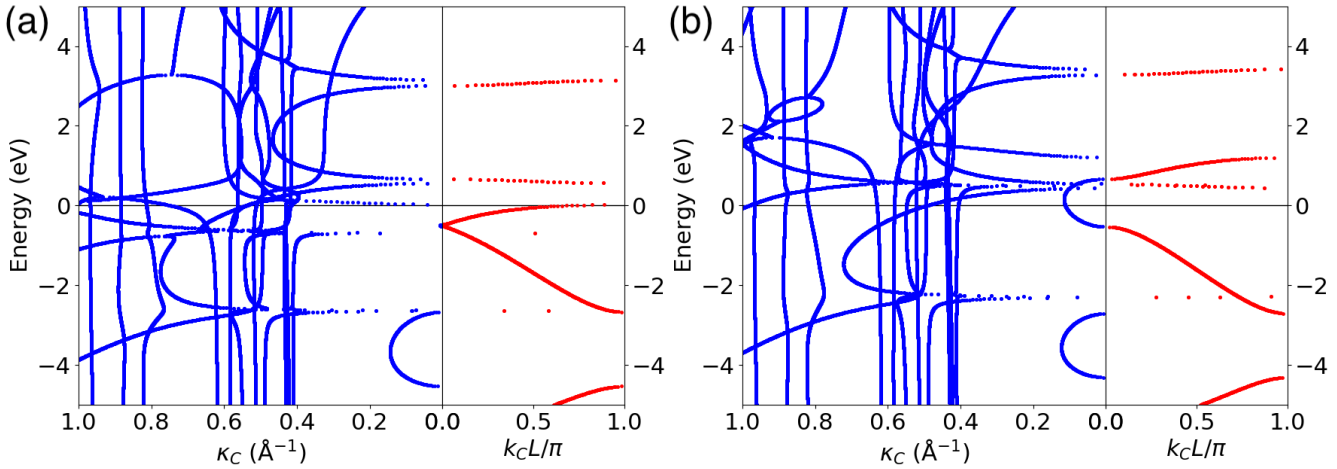

FIG. 4. (a) Spin-up and (b) spin-down complex band structures of bulk VSe_2 along the out-of-plane $\Gamma - A$ direction of the first Brillouin zone are depicted. Both the real bands (right panel) and imaginary bands (left panel) are shown.

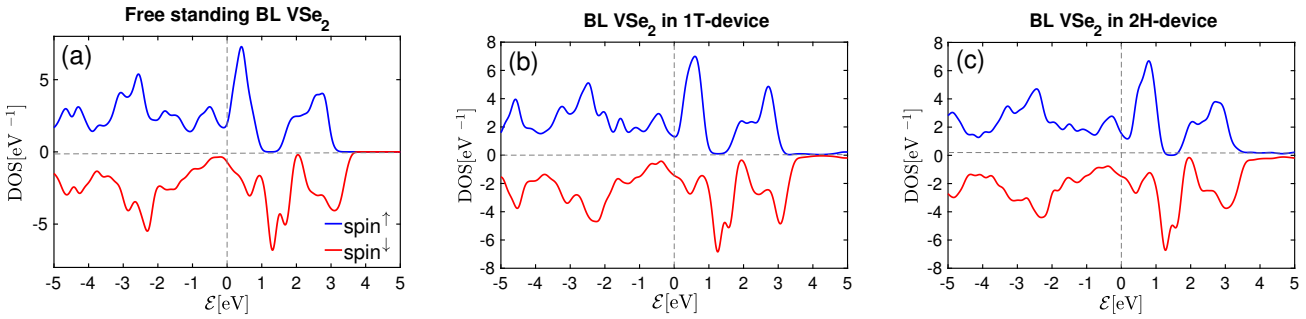

FIG. 5. (a) Electronic density of states of free-standing bilayer VSe_2. LDOS of bilayer VSe_2 when placed in the (b) 1T- and (c) 2H-device, respectively.

thin barriers. In Fig. 4a, the spin-up channel demonstrates bands crossing the Fermi level, indicative of metallic characteristics within the real parts of the band structure and suggesting active electron transport in this spin channel. Simultaneously, evanescent or decaying states are observable in the imaginary components. Conversely, Fig. 4b reveals that the spin-down channel does not feature any bands intersecting the Fermi level in the real part, pointing to a lack of metallic properties and highlighting a reliance on evanescent states for electron dynamics in this channel. This distinction emphasizes the need to take into account both real and complex wave-vector values in these analyses. Real wave-vector values correspond to periodic Bloch states that permeate the entire material, while complex wave-vector values reveal states characterized by exponential decay. Consequently, the transport properties of spin-up electrons are primarily governed by bulk-propagating states, while evanescent states are more influential in determining the transport properties of spin-down electrons.

Fig. 5 displays the local electronic density of states for bilayer VSe_2 across three different configurations: (a) free-standing, (b) sandwiched within a 1T-device, and (c) incorporated in a 2H-device setup. All panels reveal DOS peaks around the Fermi level, confirming that the metallic character of bilayer VSe_2 is preserved in device integrations. Fig. 5a highlights a significant disparity in the DOS at the Fermi level between the spin-up ($\mathrm{DOS}^{\uparrow}(\mathcal{E}=0)=1.96\,\mathrm{eV}^{-1}$) and spin-down ($\mathrm{DOS}^{\downarrow}(\mathcal{E}=0)=0.71\,\mathrm{eV}^{-1}$) channels, demonstrating enhanced spin polarization in the free-standing bilayer VSe_2. In contrast, Fig. 5b shows the DOS within a 1T-phase device where the difference between the spin channels narrows, with the spin-down channel ($\mathrm{DOS}^{\downarrow}(\mathcal{E}=0)=1.43\,\mathrm{eV}^{-1}$) slightly surpassing the spin-up ($\mathrm{DOS}^{\uparrow}(\mathcal{E}=0)=1.3\,\mathrm{eV}^{-1}$). In contrast, Fig. 5c reveals that in the 2H-device configuration, the spin-up DOS ($\mathrm{DOS}^{\uparrow}(\mathcal{E}=0)=1.55\,\mathrm{eV}^{-1}$) remains slightly higher than the spin-down ($\mathrm{DOS}^{\downarrow}(\mathcal{E}=0)=1.48\,\mathrm{eV}^{-1}$), closely reflecting

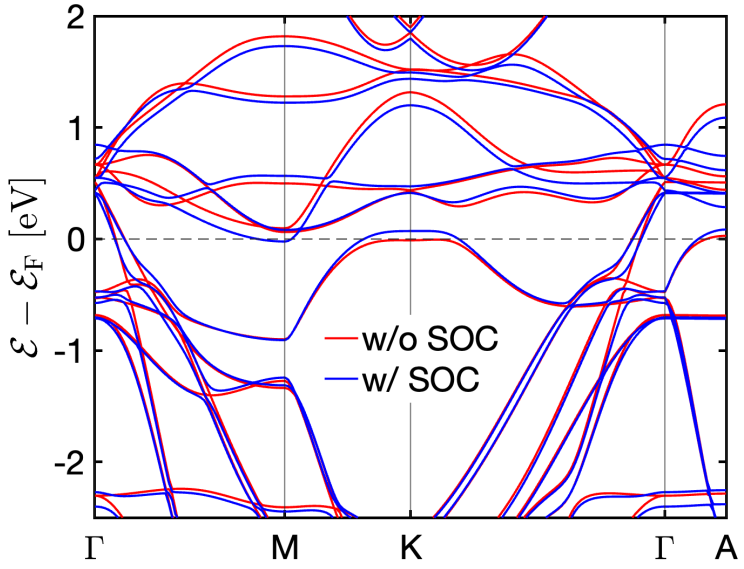

FIG. 6. Band structure of bulk VSe_2 with and without SOC.

the free-standing characteristics but with a narrowed gap between spin channels. These variations suggest that the electrode phase significantly impacts the electronic interactions within bilayer VSe_2, influencing the alignment and strength of spin polarization.

Figure 6 presents the band structure of bulk VSe_2 both with and without the inclusion of spin-orbit coupling, highlighting the substantial influence of SOC on the material's electronic characteristics. Without SOC (represented in red), the electronic bands near the Fermi level tend to overlap more significantly at the high-symmetry points K, and A within the Brillouin zone, indicating a higher degree of degeneracy. Once SOC is introduced (illustrated in blue), notable changes such as band splitting and shifts in the energy levels become apparent. This effect is especially pronounced around the M and K points where the bands not only split but also experience shifts, potentially modifying the material's electronic and optical behavior. Along the $\Gamma-A$ direction, crucial for understanding perpendicular transport properties, the plot reveals a singular dispersive band crossing the Fermi level. This band exhibits minimal influence from SOC, suggesting that it retains a well-defined spin character, crucial for applications that rely on spin transport properties.

III. MAGNETIC TUNNEL JUNCTION

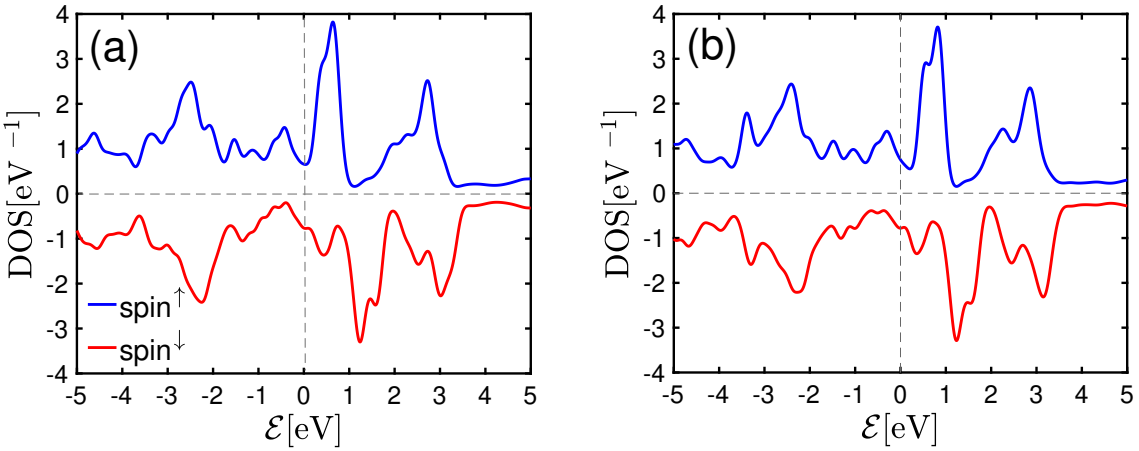

FIG. 7. The local density of states for the ferromagnetic VSe_2 layers within the MTJ setups are depicted in panels (a) for the 1T configuration and (b) for the 2H configuration.

Figure 7a and 7b showcase the local density of states for the ferromagnetic VSe_2 layers in each configuration. In the 1T-TaS_2 configuration (Fig. 7a), there is a clear disparity in the DOS between spin-up and spin-down electrons, with spin-up states exhibiting higher density near the Fermi level, indicating enhanced conduction states for spin-up electrons. In contrast, the 2H-TaS_2 configuration (Fig. 7b) shows a more balanced DOS between spin-up and spin-down states, suggesting a reduced spin polarization. Analysis of the spin-dependent density of states in the VSe_2 layers reveals a negative spin polarization at the Fermi level, measured as -8% for the 1T configuration and -2% for the 2H configuration, underscoring the influence of electrode phase on magnetic and electronic behaviors within these heterostructures.

The figure 8 displays atom-projected in-plane magneto-crystalline anisotropy energy plots for $VSe_2/MoS_2/VSe_2$ magnetic tunnel junctions sandwiched between TaS_2 electrodes, differentiated by 8a 1T and 8b 2H phase electrodes. In both configurations, the MAE shows pronounced minima at the locations of vanadium atoms, indicative of negative MAE values that align with the in-plane anisotropy for both monolayer and bulk VSe_2. This uniformity across different structural forms (monolayer, bulk, and integrated within tunnel junctions) highlights the intrinsic magnetic properties of VSe_2, primarily driven by strong spin-orbit coupling in vanadium's d-orbitals. In Fig. 8a, the MAE closely approximates that of freestanding monolayer VSe_2, reported at -0.19 meV, indicating minimal perturbation from the 1T-phase electrodes. Conversely, Fig. 8b reveals a diminished MAE when VSe_2 interfaces with 2H-phase electrodes, signifying a potential destabilization of magnetic moments within the material. This reduction in MAE suggests an increased susceptibility to external influences, such as the electrostatic environment or structural variations induced by the different electrode phases. These observations demonstrate that the electrode phase can significantly impact the magnetic characteristics of the scattering region within the device, affecting the stability and orientation of its magnetic moments.

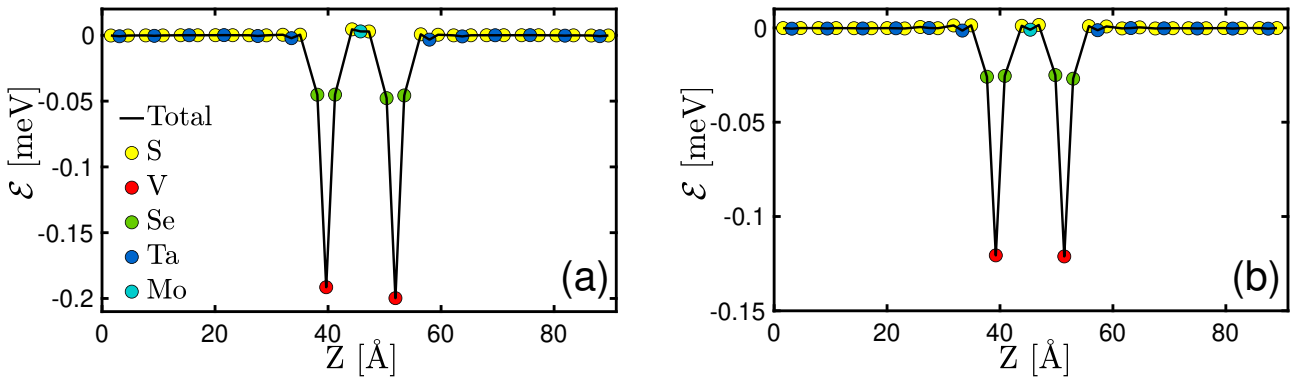

FIG. 8. Atom projected in-plane magnetocrystalline anisotropy energy plots for $VSe_2/MoS_2/VSe_2$ magnetic tunnel junctions sandwiched between TaS_2 electrodes with (a) 1T phases and (b) 2H phases.

REFERENCES

[1] M. G. Reuter, A unified perspective of complex band structure: interpretations, formulations, and applications, Journal of Physics: Condensed Matter **29**, 053001 (2016).

[2] W. Kohn, Analytic properties of bloch waves and wannier functions, Phys. Rev. **115**, 809 (1959).